Available online at www.sciencedirect.com
ScienceDirect
Polymer 48 (2007) 6294–6303
polymer
www.elsevier.com/locate/polymer

Evolution of the morphology and the mechanical properties of ternary PE/PA6/GF composites during annealing

Plamen G. Malchev [a,b,*], G. de Vos [a], B. Norder [a], Stephen J. Picken [a,b], Alexandros D. Gotsis [b,c]

[a] *Delft University of Technology, Department of Polymer Materials and Engineering, Julianalaan 136, 2628 BL Delft, The Netherlands*
[b] *Dutch Polymer Institute, P.O. Box 902, 5600 AX Eindhoven, The Netherlands*
[c] *Technical University of Crete, Department of Sciences, 73100 Chania, Greece*

Received 9 July 2007; received in revised form 7 August 2007; accepted 13 August 2007
Available online 21 August 2007

Abstract

Ternary composites have been prepared via simultaneous melt extrusion of polyethylene (PE), polyamide-6 (PA6) and short glass fibres in a twin screw extruder. If the fibres are compatible with PA6 a network of fibres welded by domains of the minor PA6 phase is build within the matrix (PE) during the processing. Although a small amount of PA6 is added, the presence of the fibres promotes the continuity of this phase. Thus, the ternary mixture resembles the morphology of a co-continuous binary blend. In this paper the stability of the ternary composites upon annealing at temperatures above the melting of PA6 is studied. An increase of the dynamic tensile modulus is observed. Contrary to the behaviour of co-continuous binary blends, for which the properties often deteriorate due to morphology coarsening, in the ternary composites, it leads to the creation of stronger contacts between the fibres and better mechanical performance. This behaviour is accounted for by a recently developed mechanical model.

Keywords: Short fibre reinforced thermoplastic blends; Fibre network; Capillary instabilities during annealing

1. Introduction

Solid fillers are often added to immiscible polymer blends, thus forming a ternary composite, to modify their properties. The properties of the blends and the corresponding ternary composites are closely related to their morphology [1–4]. The addition of a solid filler can have different impact on the morphology of the immiscible polymer blends and may lead to: (i) blend compatibilisation, due to specific interaction of the filler with both polymeric components [5–8]; (ii) filler accumulation in one phase, due to preferential interaction with this component [9–12]; or (iii) morphology alteration due to the change of the viscosity ratio [9] or due to the shape restrictions imposed by the filler particles [13,14].

During the manufacturing of immiscible polymer blends and/or ternary composites often non-equilibrium intermediate (micro-)structures are obtained. Upon further annealing of the system the morphology changes toward a state closer to the thermodynamic equilibrium. There are several studies on the stability of bi-continuous blends during their annealing [15–21]. A transition from co-continuous to dispersed morphology or v.v. is possible. In both situations, however, a decrease of the tensile modulus is reported when the continuity of the component with the higher modulus and the higher glass transition (or melting) temperature is lost [15,20]. Fewer studies have been published on the stability of ternary composites. Si et al. [8] reported that the addition of organoclay to PS/PMMA, PC/SAN and PMMA/EVA blends prevented the coarsening and the loss of co-continuity of the phases upon

* Corresponding author. Delft University of Technology, Department of Polymer Materials and Engineering, Julianalaan 136, 2628 BL Delft, The Netherlands. Tel.: +31 15 2788013; fax: +31 15 2787415.
E-mail address: p.g.malchev@tudelft.nl (P.G. Malchev).

0032-3861/$ - see front matter © 2007 Elsevier Ltd. All rights reserved.
doi:10.1016/j.polymer.2007.08.037

annealing. Zhang et al. [12] reported an improvement of the conductivity of ternary composites consisting of carbon fillers and HDPE/PMMA or HDPE/iPP upon annealing above their melting point. This was due to agglomeration and flocculation of the conductive filler. Persson and Bertilsson [14] reported an increase of the storage and loss moduli of ternary composite melts of PIB/PE and SAN/PA6 with aluminum borate whiskers upon annealing. This depended also on the (rheological) history of the samples and was correlated to some morphological changes.

Recently, complex composite materials (containing short fibre reinforcement) have also been thoroughly studied because of their potential to fine tune the final material properties by varying their composition [22,23]. Fu et al. [23] studied the effect of the polymer ratio on the mechanical properties of short glass fibre reinforced and rubber-toughened PA-6.6/PP blends. It was demonstrated that at intermediate polymer ratios composites with optimal performance are obtained, regarding not only the increase of their tensile and flexural modulus, but also the improvement of the ultimate composite properties. In the present work we analyse the effect of annealing of similar (ternary) composites on their morphology and mechanical properties. The composites comprise two immiscible thermoplastic polymers, polyethylene (PE) and polyamide-6 (PA6), mixed in volume ratios corresponding to a matrix-droplet morphology, and short glass fibre (GF) reinforcement. Such short fibre reinforced thermoplastic blends (SFRBs) have been investigated earlier regarding their morphology, rheology and mechanical properties. A preferential encapsulation of the fibres by the higher affinity or lower viscosity polymer component has been reported [24–26]. Malchev et al. [27] reported that in PE/PA6/GF ternary blends the preferential wetting of the fibres by the minor polymeric component (PA6) promotes the formation of a continuous network of fibres welded by this component. Immiscible PE/PA6 blends containing dispersed phase compatible glass fibres (GF1) sustained unusually high levels of the tensile modulus at temperatures above the melting point of the matrix phase (PE) in contrast to blends containing matrix-compatible fibres (GF2). This was attributed to the differences in their network state.

A model for the mechanical properties of a SFRB has been developed based on the deformation modes of a representative junction point of the network [27]. The model parameters are summarised in Fig. 1. Despite the fact that the properties of short fibre reinforced polymers are often strongly influenced by the fibre length distribution and orientation [28] in the present case there is no direct relation between the modulus and the fibre length. Instead, the elastic modulus is dependent on another parameter, which is the average distance, $2l$, between the two network junctions (along the fibre length). Providing that the matrix is soft enough (which is valid at temperatures around its melting point) and that the length of a single fibre, $2l_f$, is much larger than the average length between two junction points (a condition fulfilled for the composites studied here $2l_f \approx 500\ \mu m \gg 2l \approx 80\ \mu m$) the modulus of the network within the frame of the model is uniquely determined by the distance between the neighbouring junction points.

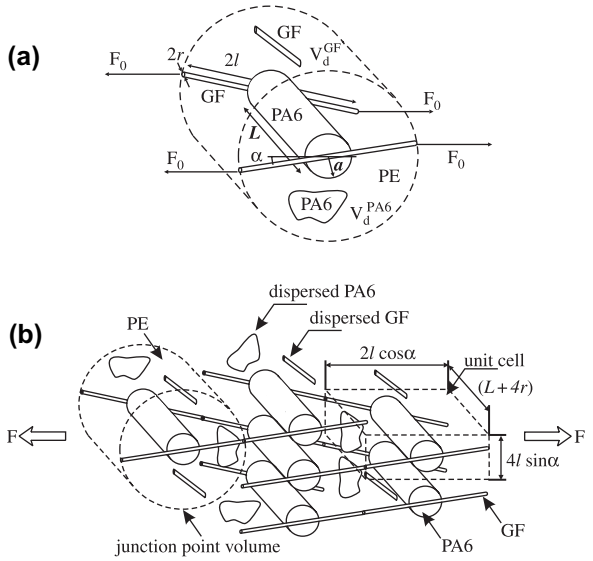

Fig. 1. (a) Structure of a junction point and the definition of the parameters; (b) PA6/GF network construction from a single repeating unit cell. F_0 represents the part of the external force, F, that acts on a single junction point [27].

Therefore, accurate knowledge of the fibre length distribution is not required.[1] In the model each junction point consists of two fibres connected by a cylindrical domain of the dispersed polymeric phase and the surrounding matrix [Fig. 1(a)]. The blend itself is considered as an assembly of these junctions [Fig. 1(b)].

Using the model, the storage modulus of the short fibre reinforced blend, E', can be expressed as a function of the temperature, T:

$$E'(T) = E'_{PE}(T) + \frac{2\pi r^2}{4(L+4r)l\sin\alpha\cos\alpha}\left[E'_0(T) - E'_{PE}(T)\right]. \quad (1)$$

Here $E'_{PE}(T)$ expresses the temperature dependence of the matrix modulus and r denotes the radius of the glass fibres. For the definition of the other parameters see Fig. 1 and the text below. The junction point modulus, $E'_0(T)$, accounts for three separate deformation processes: fibres stretching, fibres bending, and polymers twisting (for details see Ref. [27]). The last term in particular is sensitive to the volume of the PA6 welding domain [i.e., the length L and the radius a of the cylinder,

[1] Fibre length distribution is not important within the present model since the fibres are considered to be pinned at every network junction point. It is a realistic assumption only when the relative stiffness of the matrix is below, or at maximum comparable to the network stiffness. It is clear from the experimental data shown in the current article that the low temperature modulus of the investigated ternary composites is practically not influenced by the presence of the network. As it will be shown in another publication at this limit fibre length distribution indeed becomes relevant and the dependence of the modulus on the fibre content can be predicted correctly by, e.g. the shear lag model. In the present work, however, we are mostly concerned with the variations of the modulus that occur in the "second plateau" (i.e., above the melting point of the matrix) caused by the annealing. Therefore, fibre length distribution is not essential for the interpretation of the results.

Fig. 1(a)], therefore, varying L and a the model can be fitted to the experimental data and information about the state of the PA6/GF network can be obtained. The parameters characterising the morphology of the ternary composites include the average angle, 2α, between two ''welded'' fibres and the average distance, $2l$, between two neighbouring junction points along the fibre; the amounts of the dispersed phase, κ_{PA6}, and glass fibres, κ_{GF}, not incorporated within the network structure; the average length, L, and radius, a, of the connecting (PA6) cylindrical domains; and the average number of the junction points, N_{jp} (Fig. 1). Four of these parameters are independent and only three of them (l, α and κ_{PA6}) were used for the fit. As reasoned in Ref. [27] it is assumed that all the glass fibres participate in the network, i.e., $\kappa_{GF} = 0$.

2. Materials and processing conditions

The ternary composites have been prepared from two low density polyethylene grades Stamylan LD2102 (PE1) and Stamylan LD2100 (PE2) (SABIC Europe). The melting point of both grades was 110 °C, they had a tensile modulus of 250 MPa at 25 °C, but their viscosities were different (Fig. 2). A polyamide-6 (PA6) (Akulon K222D, delivered by DSM) was used as a dispersed phase. Its melting point was 220 °C and it had a tensile modulus of 2 GPa at 25 °C. The short glass fibres were provided by PPG Industries. They had a tensile modulus of 72 GPa and were compatible either to the PA6 phase (PPG3545: ϕ10 μm, 4.5 mm length) or to the PE phase (PPG3299: ϕ13.7 μm, 3 mm length), denoted here as GF1 and GF2, respectively. The PA6 component was dried in a vacuum oven at 80 °C for at least 24 h prior to use, whereas the rest of the components were used as delivered.

Ternary (70/15/15 PE/PA6/GF) and binary (85/15 PE/GF) mixtures of a fixed composition were investigated. Similar to Ref. [27] the mixtures are denoted here by the volume fractions of the components (in %) followed by the types of the components. For example, the binary mixture (composite), containing 85 vol.% of the lower viscosity polyethylene and 15 vol.% of the PA6 compatible fibres, is denoted as 85/15 PE1/GF1; whereas a ternary mixture (composite, SFRB), containing 70 vol.% of the higher viscosity polyethylene, 15 vol.% of the PA6 component and 15 vol.% of the PA6 compatible glass fibres, is denoted as 70/15/15 PE2/PA6/GF1.

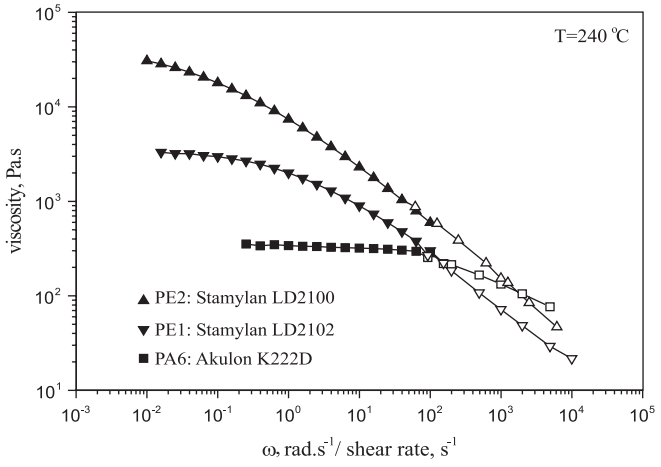

Fig. 2. Viscosity curves of the components measured at 240 °C. Closed symbols: complex shear viscosity as a function of the frequency (RMS 800 rotary rheometer in plate–plate configuration; plate diameter of 25 mm and gap of 2 mm). Open symbols: shear viscosity as a function of the shear rate (Rosand RH 7/8-2 capillary rheometer).

The viscosity curves of the components at the processing temperature (240 °C) are shown in Fig. 2. PA6 has the lowest viscosity up to about 100 s^{-1}. Between 100 s^{-1} and 3000 s^{-1} the viscosity of PE1 becomes the lowest, while the one of PE2 remains higher than that of PA6. Above 3000 s^{-1} the viscosity of PA6 becomes the highest. Since the shear rate realised during the mixing was about 230 s^{-1}, different morphologies are expected for the composites prepared with PE1 or PE2 as the matrix [31].

A co-rotating, fully intermeshing twin screw extruder (Werner & Pfleiderer ZSK-D28) with a barrel diameter of 28 mm was used to mix the components. It was operated at very low speed (20 rpm) to minimise the breakage of the fibres. The temperature in the mixing section was 240 °C (at this temperature both polymeric components are molten) and 260 °C at the cylindrical exit die (ϕ2 mm). The extrudates were immediately cooled in water and collected on a rotating roll, then dried in a vacuum oven at 80 °C and kept there until further use. Their homogeneity was very good, with only moderate breakage of the fibres: the fibre length after extrusion was approximately 500 μm.

Preserving their parallel orientation, the extrudates were compacted in flat plates ($30 \times 30 \times 2$ mm^3) using a hot press for 15 min. The press was heated to 190 °C (thus, the PA6 component was still frozen while pressing) and therefore, the morphology of the sample was preserved as formed in the extruder. These plates were further annealed at 250 °C for different times. Rectangular specimens of approximate dimensions $15 \times 2.5 \times 2$ mm^3 were punched out of them and used for the dynamic mechanical analysis.

3. Measurements

3.1. Annealing

Annealing was performed in a Mettler FP82HT hot stage under nitrogen atmosphere. The hot stage and nitrogen were preheated to the annealing temperature. Despite the precautions, a thermal degradation of the material was already obvious after 900 s of annealing, which sets the upper limit for the experiments.

The plates obtained from the press were first heated at 190 °C for 600 s using a 2 mm spacer to remove any frozen mechanical stresses within the matrix. Then different plates were subsequently annealed at 250 °C for 30 s, 90 s, 180 s, 390 s, 600 s and 900 s. After annealing, the plates were cooled down in the open air to room temperature, ensuring about the same thermal history for all of them. A mini thermocouple pushed through a small hole in the middle of a sample

revealed that the prescribed temperature reached the centre of the sample within about 60 s. Thus the samples annealed for 30 s and 90 s were non-uniformly heated and perhaps only partial melting of the material was realised for them.

3.2. Dynamic mechanical analysis (DMA)

A Perkin–Elmer 7e Dynamic Mechanical Analyser was used for the characterisation of the mechanical properties in tensile mode. A static and a dynamic force (at a frequency of 1 Hz) were imposed on the rectangular specimens punched out of the annealed plates. During the measurement a dynamic control ensured a constant amplitude of 5 μm (~0.05% strain amplitude), and a tension control ensured that the static force always exceeded the dynamic by 10%. The storage, E', and the loss, E'', tensile moduli were monitored during a temperature sweep test, starting at room temperature (20 °C) and ending after the melting of the PA6 component (220 °C). The temperature was raised with a constant rate of 5 °C/min.

Since the reproducibility was not very good, multiple measurements were conducted. The poor reproducibility can be due to compositional variations originating from the sample preparation technique. While punching out a sample of the annealed plates, a single extrudate strand or a boundary between two extrudates can form the major part of the volume of the sample. Although, it has been reported that core–skin morphology in ternary mixtures is less pronounced than in their binary equivalents [24,25] a different degree of fibre orientation was observed in the skin and the core of injection molded specimens. This could result in some variation in the mechanical properties of the samples. Another reason for poor reproducibility could be the degradation of the composites, despite that measures preventing the oxidation were taken. However, the observed trends were repeatable during multiple tests and the results presented here are characteristic for the SFRBs.

4. Results and discussion

The mechanical properties of SFRBs containing different glass fibre and PA6 loadings have been analysed elsewhere [27]. A network of fibres welded together by the dispersed (PA6) phase is formed during the mixing and/or the consequent sample manipulation. The presence of the PA6/GF network results in a second plateau in the log $E'(T)$ and log $E''(T)$ curves. This plateau is situated above the melting temperature of the matrix component and is absent in the binary PE/GF composites.

Figs. 3 and 4 show the tensile storage modulus, E', plotted as a function of the temperature, in a semi-logarithmic plot, for samples that have been annealed for different time intervals. The curves shown in the figures are the logarithmic averages of 2–3 separate measurements. The two plateau regions are easily recognised for these SFRBs, based on PA6 compatible fibres (GF1). The first plateau spreads up to the melting point of the matrix (PE) at 110 °C. The second plateau, which is lower than the first, spreads between 110 °C and 220 °C, until the second dispersed thermoplastic component (PA6) melts.

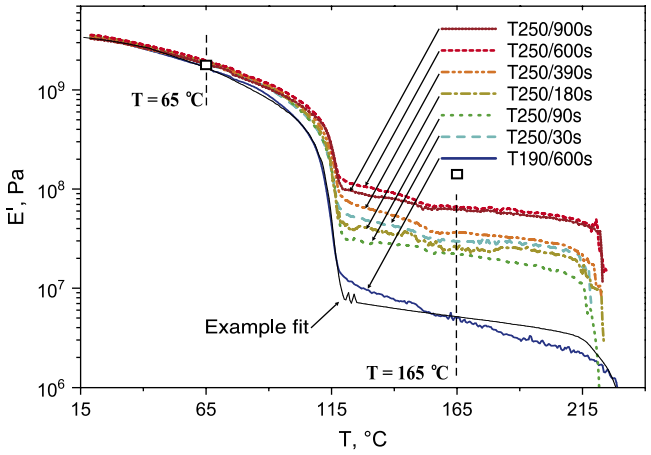

Fig. 3. Dynamic tensile modulus, E', as a function of the temperature measured in DMA at 5 °C/min for 70/15/15 PE1/PA6/GF1 ternary blends annealed for different times. The modulus was monitored by small oscillations of 0.05% amplitude. Each curve is the average of 2–3 separate measurements. An example fit of the modulus with the model reported in Ref. [27] is also shown for the non-annealed sample. The quality of the fits for the annealed samples improves, as can be judged by the similarity in the slopes of the model prediction and the modulus measured for the annealed samples. The open squares correspond to the maximum predicted, final (equilibrium), composite modulus (Table 5).

With the melting of the PA6 phase the samples collapse. The loss modulus (not shown) follows the same general trend, but the drop around the melting temperature of PE is smaller. Overall, annealing of the samples results in an increase of the second plateau modulus.

In the SFRBs containing GF2 (not shown here) the second plateau is not easily reproduced. These samples fail at temperatures somewhat above 110 °C that can be associated to the inability of a proper fibre network to be formed within them. The second plateau, whenever it appears in this case, is not affected by annealing or decreases slightly with the annealing time.

The variation of the storage and the loss moduli with the annealing time [$E'(t)$ and $E''(t)$] can be seen more clearly

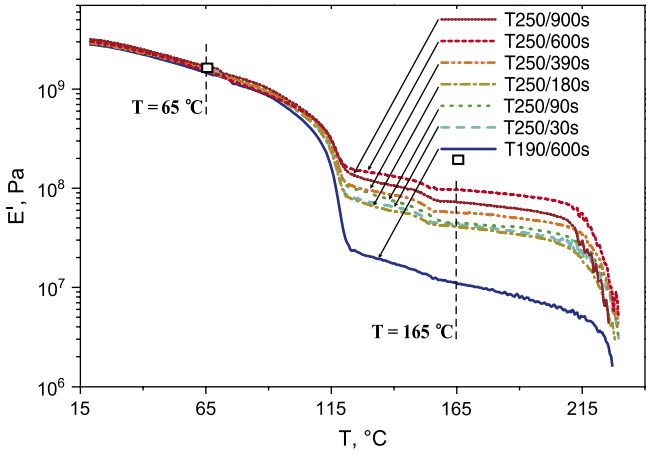

Fig. 4. Dynamic tensile modulus as in Fig. 3, for the ternary blends containing 70 vol.% PE2 (higher viscosity PE), 15 vol.% PA6 and 15 vol.% GF1 annealed for different times. The open squares correspond to the maximum predicted, final (equilibrium), composite modulus (Table 5).

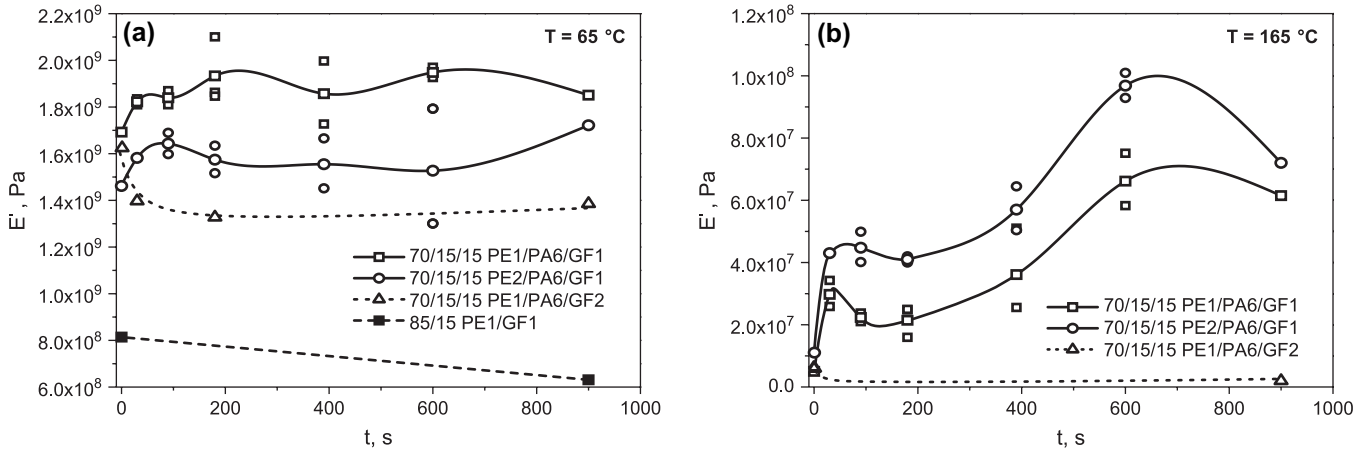

Fig. 5. Storage modulus variation with the annealing time: (a) at ~65 °C (in the middle of the first plateau region) and (b) at ~165 °C (in the middle of the second plateau). Lines are to guide the eye.

from Figs. 5 and 6, respectively. Part (a) of the figures shows the variation of the modulus in the middle of the low temperature plateau (at 65 °C) vs. the annealing time. Part (b) shows the variation of the modulus at the middle of the high temperature plateau (at 165 °C).

When the annealing time is increased, the moduli (E' and E'') of the SFRBs containing GF1 increase slightly in the middle of the first plateau (at 65 °C). The storage modulus of the composite containing PE1 is slightly higher than that of the one containing PE2. In this region the blend containing GF2 shows a decrease of the storage modulus with the annealing time. The loss modulus shows similar trends. The variations, however, are generally small and comparable to the accuracy of the test [Figs. 5(a) and 6(a)].

The change in the moduli with the annealing time at the second plateau is much more pronounced, covering an order of magnitude [Figs. 5(b) and 6(b)]. The composites containing GF1 show an initial rapid increase of the storage modulus. A local maximum is reached. Then, E' drops to a local minimum. The minimum is reached earlier for the composite containing PE1 ($t \approx 130$ s) than for the composite containing PE2 ($t \approx 180$ s). Leaving out the considerations of the last points (annealed for 900 s), due to sample degradation, a final steady increase of the modulus for both SFRBs is observed. Although, the scatter of the loss modulus data is somewhat larger, they follow the same trend with a shift in time. Roughly, a maximum is observed, at around the minimum of the storage modulus. For the composite containing GF2 only two points (0 s, 900 s) could be extracted for the second plateau region, and they reveal a small decrease of the storage and loss moduli during annealing.

The data of an equivalent binary composite (85/15 PE1/GF1) with the same fibre loading as in the ternary blends are also included in the figures for comparison [the dashed lines in Figs. 5(a) and 6(a)]. The small decrease of the moduli in this case can be attributed to some degradation of the sample.

The observed trend of the binary composite confirms that the variation of the modulus of the SFRBs is not related to the degradation of the matrix (PE) and must be attributed entirely to the changes in the state of the PA6/GF network during annealing. The variations of the storage modulus with the

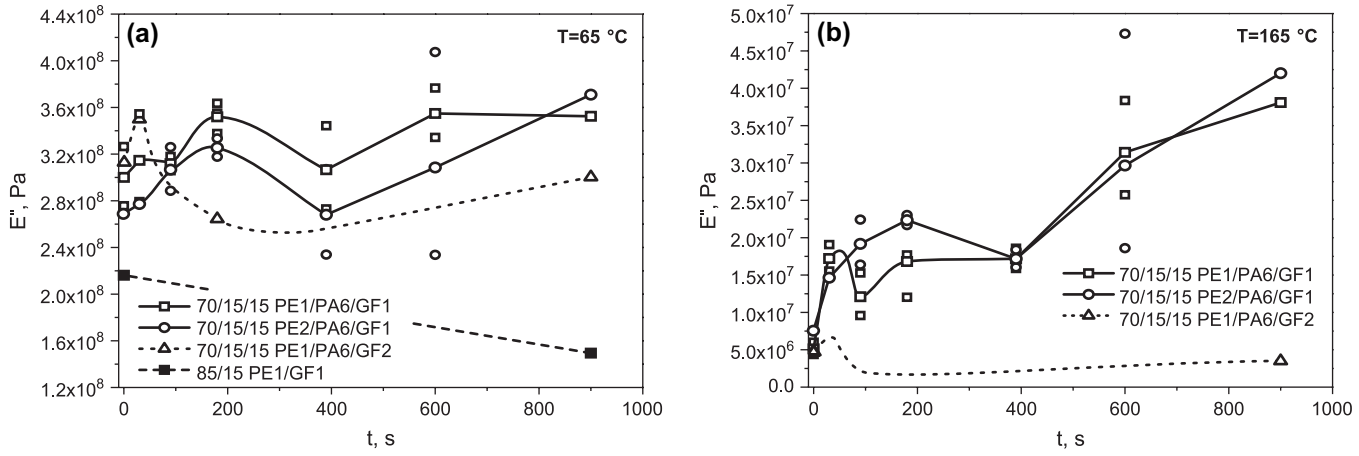

Fig. 6. Loss modulus variation with the annealing time: (a) at ~65 °C (in the middle of the first plateau region) and (b) at ~165 °C (in the middle of the second plateau). Lines are to guide the eye.

Table 1
Fitting data for the 70/15/15 PE1/PA6/GF1 composites

Annealing time	Fitting parameters			Structural parameters		
t, s	α, °	l, μm	κ_{PA6}	a, μm	L, μm	N_{jp}, mm^{-3}
0	9.45	29.60	0.773	4.36	35.47	16 131
30	10.30	30.20	0.433	7.65	29.29	15 811
90	10.05	30.95	0.575	6.70	29.24	15 432
180	9.73	31.50	0.550	6.86	29.98	15 175
390	10.60	30.75	0.440	7.99	27.39	15 528
600	9.85	30.75	0.165	9.16	30.52	15 528
900	10.30	31.20	0.290	8.94	27.70	15 303

The values reported in the table are obtained averaging the parameters from all individual fits.

annealing time can be related to the SFRB morphology development using the mechanical model introduced above. The storage modulus data obtained at different annealing times (Figs. 3 and 4) are fitted to the mechanical model, Eq. (1), within the whole temperature interval. An example fit of the $E'(T)$ dependence can be seen in Fig. 3. The averaged values of the fitting and the structural (i.e., generated by the model) parameters are collected in Tables 1–3. The model parameters a and L (characterising the morphology of the PA6 phase that participates in the network) are also plotted in Fig. 7 as a function of the annealing time t.

The radius of the PA6 cylindrical domains, a, varies with the annealing time in a similar manner to the storage modulus of the corresponding SFRB taken in the middle of the second plateau [Fig. 7(a) vs. Fig. 5(b)]. This is expected, because the network structure is entirely responsible for the presence of the second plateau. The overall increase of the radius of the PA6 domains connecting the fibres with the annealing time reflects the coarsening of the PA6 morphology.

During the processing of the blends a thin PA6 layer (~1 μm) builds around the surface of the glass fibres, especially for the PA6 compatible GF1. This layer can be seen in the optical micrograph taken before annealing (the inclusion in Fig. 8, top). Similar observations have been made also for other ternary composites [24,25,29,30]. The minor, lower viscosity phase, can be driven to the fibre surface if the processing conditions are appropriate [31] or if such distribution promotes the continuity of the phase [14]. Both conditions are satisfied here. The thickness of the layer depends on the viscosity and the volume ratio of the polymeric components,

Table 2
Fitting data for the 70/15/15 PE2/PA6/GF1 composites

Annealing time	Fitting parameters			Structural parameters		
t, s	α, °	l, μm	κ_{PA6}	a, μm	L, μm	N_{jp}, mm^{-3}
0	12.50	28.80	0.720	5.92	23.02	16 579
30	11.80	28.70	0.350	8.54	25.57	16 636
90	12.85	29.25	0.440	8.77	21.28	16 185
180	12.55	28.75	0.430	8.45	22.97	16 464
390	12.60	28.75	0.315	9.28	22.81	16 521
600	12.45	28.65	0.070	10.62	23.60	16 695
900	12.00	28.00	0.080	9.96	25.98	16 753

The values reported in the table are obtained averaging the parameters from all individual fits.

Table 3
Fitting data for the 70/15/15 PE1/PA6/GF2 composites

Annealing time	Fitting parameters			Structural parameters		
t, s	α, °	l, μm	κ_{PA6}	a, μm	L, μm	N_{jp}, mm^{-3}
0	10.00	40.00	0.740	6.63	44.43	6360
30	10.00	39.00	0.860	4.71	46.28	6523
180	10.00	38.00	0.860	4.55	48.21	6694
900	9.50	39.00	0.860	4.53	50.00	6523

as well as, on the processing conditions. At fixed composition a thicker layer is formed in the case of a higher viscosity matrix, for which not only the interfacial interactions, but also the viscosity difference favours the build-up of the layer.

Before annealing, the junction points of the network are relatively weak. They contain only a small amount of the PA6 phase, found between the crossing fibres (Fig. 8, top). Therefore, their average radius is similar to the radius of the fibres, $a(0)/r \approx 1$ (Fig. 7). With the liquefying of PA6 above 220 °C the layer becomes unstable and redistribution of PA6 material around the junction points occurs (Fig. 8, bottom). This is driven by two processes, both minimising the interfacial energy of the PA6 layer. The first is *Rayleigh instability of an annular liquid layer surrounding a fibre surface*. Different aspects of this process were studied by Refs. [32–37]. The second process is the process of PA6 retraction toward the corners formed at the crossing points of the fibres, where the minimisation of the interfacial energy of the PA6 layer is most effective. Similar accumulation of a liquid has been reported in curved microchannels [38].

The first process is akin to the classical process of Rayleigh instability of a liquid jet (where a solid fibre is not present). This process has been theoretically analysed for non-viscous surrounding media [39] and for two viscous liquids [40]. A corresponding treatment for *Rayleigh instability of an annular liquid layer surrounding a fibre surface* has been done in the case of non-viscous surrounding media (i.e., air). The presence of the fibre introduces extra boundary conditions and complicates the analysis, e.g. [32]. As a consequence the transition from non-viscous to viscous surrounding is not trivial and, to our knowledge, a theoretical description of the process for viscous surrounding media does not exist.

Another observation that deserves a comment is the initially very rapid increase of the junction point radius for the SFRBs containing GF1 and the local peak in Fig. 7(a). This behaviour was observed in multiple tests with relatively small variations from batch to batch and it is considered to be real. Many factors could contribute to its origin. A possible scenario for the development of the morphology that can explain this behaviour is provided in the following. We consider the binding PA6 cylindrical domains as belonging to one of the following three categories. In each of them the PA6 linkages undergo changes that result from different processes and contribute in a specific manner to the value of the modulus.

(1) A part of the PA6 bridges will undergo an initial retraction, driven by the interfacial energy minimisation or the relaxation of frozen mechanical stresses. The radius of these

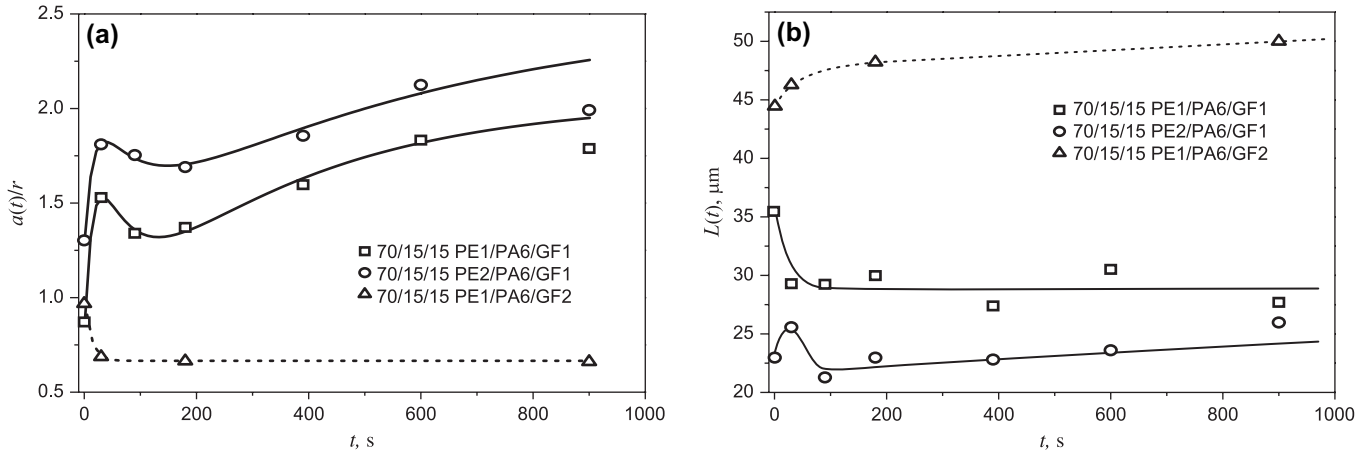

Fig. 7. (a) Time evolution of the radius of the welding cylinders (normalised to the fibre radius) obtained after fitting the data from Figs. 3 and 4 to the mechanical model [27]. The lines are fits according to Eq. (2). (b) The evolution of the length of the welding cylinders again obtained after fitting the data to the model. Lines are to guide the eye.

domains will increase, while their length will decrease [Fig. 7(b)]. This will result in an initial increase of the storage modulus.

(2) The relaxation of the mechanical stresses will stretch the bridges from the second category. They will become unstable and will consequently undergo a break-up process (Rayleigh instabilities of a jet). This is accompanied with a decrease of the storage modulus and an increase of the loss modulus [Figs. 5(b) and 6(b)].

(3) The major part of the PA6 domains will be those that increase their radius due to the process introduced above, i.e., *Rayleigh instability of an annular liquid layer surrounding a fibre surface*. This is a much slower process and must result again in an increase of the storage modulus [Fig. 5(b)].

The shape of the curve in Fig. 5(b) can be described by the sum of the contributions of the three processes, each of which has a different magnitude and time constant. The first process is expected to be very rapid, as it originates most probably from the relaxation of frozen mechanical stresses. Thus, initially one will have an increase of the modulus and the average radius of the junction point, due to process (1). Then, process (2), the breaking of the unstable PA6 domains, starts to dominate. It results in lowering of the number of the junction points, and therefore, in the decrease of the storage modulus. This process is associated with the loss of elastically stored energy and leads to an increase of the loss modulus. It is also viscosity dependent. Therefore, the minimum of the storage modulus (maximum of the loss) is delayed for the higher viscosity matrix. Fitting the storage modulus with the mechanical

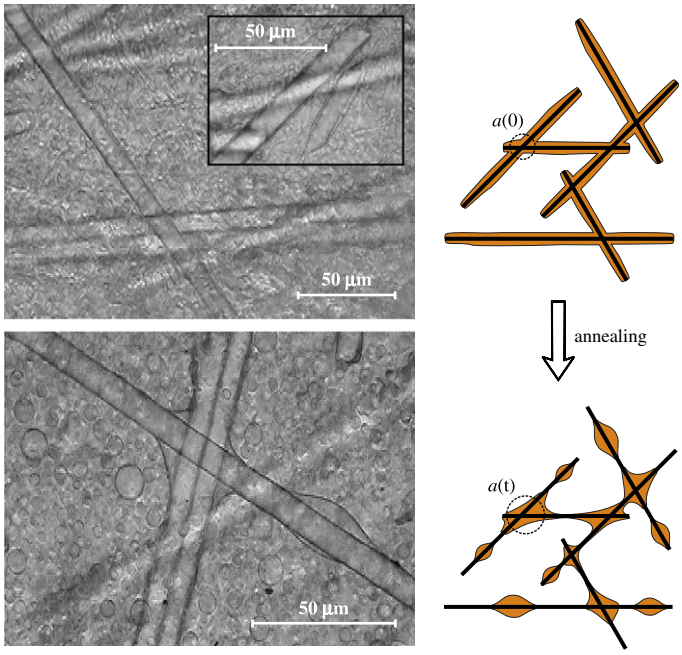

Fig. 8. Composite morphology before (top) and after (bottom) annealing. The optical micrographs are taken from a sample with lower GF concentration: 80/15/05 PE1/PA6/GF1.

model, gives an effective decrease of the average radius of the junction points. The third process, *Rayleigh instability of an annular liquid layer surrounding a fibre surface*, has the highest time constant. It prevails at long annealing times and increases both the average junction point radius and the modulus.

To give form to the above arguments we express the radius of the PA6 cylinder as a function of the annealing time, $a(t)$ [Fig. 7(a)], as a sum of three Debye processes corresponding to the ones described above:

$$a(t) = a_0 + a_1\left(1 - e^{-t/\tau_1}\right) + a_2\left(1 - e^{-t/\tau_2}\right) + a_3\left(1 - e^{-t/\tau_3}\right). \quad (2)$$

Here a_0 is the initial radius; a_1, a_2 and a_3 are the contributions to the radius growth of the three processes; and τ_1, τ_2 and τ_3 are the corresponding time constants. A similar form, but with one exponent, was used to describe the increase of the conductivity in conductive ternary composites [12].

The curves of Fig. 7(a) were fitted with Eq. (2). The fitting procedure was conducted in two steps. The data points for 30 s and 90 s annealing time were initially given zero weight and fitting was performed to obtain a value for the time constant of the slowest process, τ_3. The parameter τ_1 was arbitrarily set to 15 s because it accounts for the fast relaxation of the mechanical stresses. The other parameters were evaluated from the best fit of the complete data set. The values of the variables are presented in Table 4. This table indicates that processes (2) and (3) are distinctly decelerated when the higher viscosity matrix is used.

The process that seems to be dominating the enhancement of the modulus upon annealing for long time is that of the *Rayleigh instability of an annular liquid layer surrounding a fibre surface*. This has been studied for the case of non-viscous media surrounding the coated fibre [32]. The break-up rate, Q, for a viscosity dominated process was estimated as:

$$Q(k) \approx \frac{\Gamma\left(1 - k^2r^2\right)k^2h^3}{3\eta_0 r^2}, \quad \text{if } h \ll r,\ \rho Q h^2/\eta_0 \ll 1 \quad (3)$$

where $k < 1/(r+h)$ is the wave vector of the instability; Γ is the liquid/air interfacial tension; η_0 and ρ are the zero shear rate viscosity and the density of the film forming liquid, respectively; r is the fibre radius; and h is the film thickness. The maximum of the break-up rate, Q_{max}, determines the wavelength, $2\pi/k_{max}$, of the dominant instability responsible for the break-up of the liquid annular layer and provides an estimate for the time constant of the process, i.e., $\tau_3 \approx 1/Q_{max}$. The above should hold also for the more complicated case of a viscous medium surrounding the film. By reason of similarity to the Rayleigh instability of a liquid jet, the viscosity ratio of the liquids is expected to play some role. Although an actual relation between the variables and the time scale of the process was not found in the literature, one can expect that the increase of the viscosity of the surrounding medium will slow down the break-up process. Obviously, the time scale of this process is dependent not only on the viscosities, but also strongly dependent on the thickness of the layer [Eq. (3)]. Thinner layers slow down the process or even completely stabilize the film in the case of attractive interactions between the liquid and the fibre surface [41].

Extending this argument to the SFRBs analysed above, one can debate that the effects of the layer thickness and the matrix viscosity can partially compensate. As a result, the break-up rates of both composites (containing, respectively, PE1 matrix for which thinner PA6 layers are found and PE2 matrix where thicker layers are present) differ only by a factor of 2 (Table 4), despite the order-of-magnitude difference in their matrix viscosities (Fig. 2). Further, it can also be anticipated that the wavelength of the Rayleigh instabilities may be thickness dependent. Thinner layers will slow down the instability propagation, thus, shorter wavelength might be expected and, therefore, less material would be transported from the adjacent areas into the junction. In this case the composites based on the higher viscosity matrix will have a potential for higher modulus increase. The experimental results indeed suggest that the absolute increase of the storage modulus of the PE2 based composite is higher, Fig. 5(b). For correct comparison, however, an estimation of the final storage modulus of the ternary composites at infinite annealing time is needed.

Such estimation of $E'(t \to \infty)$ is provided in Table 5 and also included in Figs. 3 and 4. Whereas for the GF2 containing composites no change of the PA6 distribution is expected after long annealing times ($\kappa_{PA6} = 0.86$, Table 3), in the case of GF1 composites it is plausible to assume that at the end of the annealing process the whole PA6 amount will contribute to the network, i.e., $\kappa_{PA6} = 0$. In this case, the final composite modulus can be estimated from Eq. (1) providing that the values of the model parameters (α and l) are such as to obtain the predicted average junction point radius [Eq. (2)] at infinite annealing time, $a_\infty = a_0 + a_1 + a_2 + a_3$, Table 4. One should notice that the same value of a_∞ can be obtained with many different sets for α and l. To limit the possibilities in Table 5, the values of the parameter $l(t \to \infty)$ are taken as an average from the first 6 values listed in Tables 1–3.

The values of E' included in Table 5 are tentative. More detailed and accurate measurements of the modulus as a function of the annealing time are required to correctly establish the

Table 4
Parameters obtained by fitting Eq. (2) to $a(t)$ dependence

Composite	a_0/r	a_1/r	τ_1, s	a_2/r	τ_2, s	a_3/r	τ_3, s	a_∞, μm
70/15/15 PE1/PA6/GF1	0.87	1.26	15	−1.37	59.40	1.28	347.25	10.21
70/15/15 PE2/PA6/GF1	1.32	0.81	15	−0.83	78.90	1.22	587.18	12.60
70/15/15 PE1/PA6/GF2	0.97	0	–	−0.31	11.9	0	–	4.52

The radius of the PA6 domain at infinite annealing time is given as: $a_\infty = a_0 + a_1 + a_2 + a_3$.

Table 5
Estimation of the final (at infinite annealing time) storage modulus of the composites at $T = 65$ °C and 165 °C from Eq. (1)

Composition	Annealing time	Model parameters				$T = 65$ °C	$T = 165$ °C
70/15/15	t, s	α, °	l, μm	κ_{PA6}	$a(t)$, μm	E', GPa	E', MPa
PE1/PA6/GF1	0	9.45	29.60	0.77	4.4	1.64	5.27
	$t \to \infty$	11.00	30.63	0	10.9	1.75	138.60
PE2/PA6/GF1	0	12.50	28.80	0.72	5.9	1.45	10.67
	$t \to \infty$	14.22	28.82	0	12.6	1.57	185.90
PE1/PA6/GF2	0	10.00	40.00	0.74	6.6	1.52	5.85
	$t \to \infty$	9.50	39.00	0.86	4.5	1.47	1.91

For comparison the values of E' at zero annealing time, calculated for the model parameters listed in Tables 1–3, are also shown. The storage modulus of the final (equilibrium) morphology is estimated by introducing appropriate pairs of parameters (α and l) in the model [27], ensuring practically the same values of $a_\infty[=a(t \to \infty)]$ are obtained as listed in Table 4. For the GF1 containing composites it is assumed that all of the PA6 components contribute to the network ($\kappa_{PA6} = 0$), whereas for the composites containing GF2, $\kappa_{PA6} = 0.86$ (Table 3).

ultimate modulus increase. For this purpose a study of the morphological changes during annealing was performed using rheometry and the results will follow in another publication. In the present study, despite the fact that only limited number of data points could be obtained and no definite estimate of the mechanical properties of the final equilibrium morphology could be made, the increase of the storage tensile modulus of ternary composites upon annealing has been clearly demonstrated.

5. Conclusions

The stability of the morphology of a specific type of ternary composites (short fibre reinforced thermoplastic blends) comprised of PE matrix, PA6 dispersed (minor) phase and short glass fibre reinforcement during annealing was studied via dynamic mechanical analysis (DMA). DMA data were fit to a recently developed theoretical model [27] that relates the variations of the storage modulus to the morphological changes. Contrary to co-continuous binary blends, where the mechanical properties often deteriorate with the coarsening of the structure [20], the elasticity modulus of the ternary composites containing dispersed phase compatible fibres increases by this coarsening. The process responsible for the observed increase is governed by the Rayleigh instability of an annular film surrounding a cylindrical surface. Optical observations of an initial, non-annealed, and an annealed morphology are in good agreement with the interpretation proposed here.

Acknowledgements

This research forms part of the research programme of the Dutch Polymer Institute (DPI), project #256. The authors acknowledge PPG Industries for the delivery of the glass fibres and SABIC Europe for the supply of the PE grades.

References

[1] Willemse RC, Posthuma de Boer A, van Dam J, Gotsis AD. Polymer 1998;39(24):5879–87.
[2] Paul DR, Bucknall CB. Polymer blends, vols. 1 and 2. New York: John Wiley & Sons; 2000.
[3] Tucker CL, Moldenaers P. Annual Review of Fluid Mechanics 2002;34:177–210.
[4] Pötschke P, Paul DR. Journal of Macromolecular Science, Part C – Polymer Reviews 2003;34(1):87–141.
[5] Karim A, Liu D-W, Douglas JF, Nakatani AI, Amis EJ. Polymer 2000;41:8455–8.
[6] Nesterov AE, Lipatov YS, Ignatova TD. European Polymer Journal 2001;37:281–5.
[7] Huang Y, Jiang S, Li G, Chen D. Acta Materialia 2005;53:5117–24.
[8] Si M, Araki T, Ade H, Kilcone ALD, Fisher R, Sokolov JC, et al. Macromolecules 2006;39:4793–801.
[9] Persson AL, Bertilsson H. Polymer 1998;39:5633–42.
[10] Huang J-C. Advances in Polymer Technology 2002;21(4):299–313.
[11] Feng J, Chan C-M, Li J-X. Polymer Engineering and Science 2003;43(5):1058–63.
[12] Zhang C, Wang P, Ma C, Wu G, Sumita M. Polymer 2006;47:466–73.
[13] Benderly D, Siegmann A, Narkis M. Polymer Composites 1996;17(3):343–52.
[14] Persson AL, Bertilsson H. Polymer 1998;39(18):4183–90.
[15] Quintens D, Groeninckx G, Guest M, Aerts L. Polymer Engineering and Science 1990;30(22):1474–83.
[16] Quintens D, Groeninckx G, Guest M, Aerts L. Polymer Engineering and Science 1990;30(22):1484–90.
[17] Verhoogt H. Morphology, properties and stability of thermoplastic polymer blends. Ph.D. dissertation. Technical University of Delft, Delft; 1992.
[18] Willemse RC. Polymer 1999;40:2175–8.
[19] Veenstra H, van Dam J, Posthuma de Boer A. Polymer 1999;40:1119–30.
[20] Veenstra H, Verkooijen PCJ, van Lent BJJ, van Dam J, Posthuma de Boer A, Nijhof AHJ. Polymer 2000;41:1817–26.
[21] Yuan Z, Favis BD. AIChE Journal 2005;51(1):271–80.
[22] Fu S-Y, Lauke B, Zhang YH, Mai Y-W. Composites: Part A 2005;36:987–94.
[23] Fu S-Y, Lauke B, Li RKY, Mai Y-W. Composites: Part B 2006;73:182–90.
[24] Benderly D, Siegmann A, Narkis M. Polymer Composites 1996;17(1):86–95.
[25] Fisher I, Siegmann A, Narkis M. Polymer Composites 2002;23(1):34–48.
[26] Li CQ, Zhang Y, Zhang YX, Zhang CM. Polymers and Polymer Composites 2002;10(8):619–26.
[27] Malchev PG, David CT, Picken SJ, Gotsis AD. Polymer 2005;46:3895–905.
[28] Hull D, Clyne TW. An introduction to composite materials. 2nd ed. Cambridge: Cambridge University Press; 2000.
[29] Persson AL, Schreiber HP. Journal of Polymer Science, Part B: Polymer Physics 1997;35:2457–64.
[30] Maeng YJ, Yoon BS, Suh MH, Im WB, Lee SH. Polymer Composites 2000;21:41–50.
[31] Noh C-H, Yoon BS, Suh MH, Lee SH. Polymer 2001;42:2695–700.

[32] Dumbleton HJ, Hermans JJ. Industrial and Engineering Chemistry Fundamentals 1970;9(3):466–9.
[33] Carrol BJ, Lucassen J. Journal of the Chemical Society-Faraday Transactions I 1974;70(7):1228–39.
[34] Rosenau P, Oron A. Physics of Fluids A 1989;1(11):1763–6.
[35] Deissler RJ, Oron A, Lee YC. Physical Review A 1991;43(8): 4558–61.
[36] Yarin AL, Oron A, Rosenau P. Physics of Fluids A 1993;5(1):91–8.
[37] Kliakhandler IL, Davis SH, Bankoff SG. Journal of Fluid Mechanics 2001;429:381–90.
[38] Gau H, Herminghaus S, Lenz P, Lipowsky R. Science 1999;283:46–9.
[39] Rayleigh Lord. Proceedings of the London Mathematical Society 1878;10(4):361–401.
[40] Tomotica S. Proceedings of the Royal Society of London, Series A 1935;150:322–37.
[41] Brochard F. Journal of Chemical Physics 1986;84(8):4664–72.